Structural, electronic, and magnetic properties of single MnAs nanoclusters in GaAs

AIP | Applied Physics Letters

Structural, electronic, and magnetic properties of single MnAs nanoclusters in GaAs

E. P. Smakman, S. Mauger, D. W. Rench, N. Samarth, and P. M. Koenraad

Citation: Applied Physics Letters **105**, 232405 (2014); doi: 10.1063/1.4904097
View online: http://dx.doi.org/10.1063/1.4904097
View Table of Contents: http://scitation.aip.org/content/aip/journal/apl/105/23?ver=pdfcov
Published by the AIP Publishing

Structural, electronic, and magnetic properties of single MnAs nanoclusters in GaAs

E. P. Smakman,[1,a)] S. Mauger,[1] D. W. Rench,[2] N. Samarth,[2] and P. M. Koenraad[1]
[1]*Department of Applied Physics, Eindhoven University of Technology, Den Dolech 2, 5612 AZ Eindhoven, Netherlands*
[2]*Department of Physics and Materials Research Institute, The Pennsylvania State University, University Park, Pennsylvania 16802, USA*

(Received 1 October 2014; accepted 2 December 2014; published online 8 December 2014)

MnAs nanoclusters in GaAs were investigated with cross-sectional scanning tunneling microscopy. The topographic images reveal that the small clusters have the same zinc-blende crystal structure as the host material, while the larger clusters grow in a hexagonal crystal phase. The initial Mn concentration during molecular beam epitaxy growth has a strong influence on the size of the clusters that form during the annealing step. The local band structure of a single MnAs cluster is probed with scanning tunneling spectroscopy, revealing a Coulomb blockade effect that correlates with the size of the cluster. With a spin-sensitive tip, for the smaller clusters, superparamagnetic switching between two distinct states is observed at T = 77 K. The larger clusters do not change their magnetic state at this temperature, i.e., they are superferromagnetic, confirming that they are responsible for the ferromagnetic behavior of this material at room-temperature. © *2014 AIP Publishing LLC*. [http://dx.doi.org/10.1063/1.4904097]

Dilute magnetic semiconductors such as (Ga,Mn)As are interesting candidates for providing room-temperature ferromagnetism.[1–4] However, these materials have only been grown with a Curie temperature up to $T_C = 185$ K,[5] which is still far below room-temperature. An alternative approach is the use of nm-sized ferromagnetic clusters in a semiconductor host, e.g., MnAs nanoclusters in GaAs.[6–8] This material has recently been demonstrated to be ferromagnetic well above room-temperature[9] and the MnAs clusters have been shown to exhibit metallic behavior.[10] In this work, the aim is to investigate the MnAs nanoclusters in detail with cross-sectional scanning tunneling microscopy (X-STM) and confirm their structural, metallic, and magnetic properties at the nanoscale. For this purpose, the topography, electronic band structure, and magnetic switching of single MnAs clusters are probed with X-STM.

The samples for X-STM were grown by molecular beam epitaxy (MBE). On a [001] oriented n-doped GaAs substrate, first, a 120 nm Be-doped buffer layer was grown, with a Be concentration of around $\sim 1 \times 10^{18}$ cm^{-3}. This is followed by a low-temperature 100 nm Be:$Ga_{1-x}Mn_xAs$ layer grown at $T = 245$ °C. The final 2 nm high-temperature capping layer consists of Be:GaAs and is grown at $T = 600$ °C. We note here that the Be effusion cell temperature used for the low-temperature Be:$Ga_{1-x}Mn_xAs$ layer was 40 °C higher than that used for the high-temperature buffer and capping layers. This was done to keep the carrier concentration in all layers as similar as possible by compensating for the known double-donor effect caused by As anti-sites in low-temperature (Ga,Mn)As.[11] The last annealing step is crucial for obtaining the MnAs nanoclusters and the desired magnetic behavior. The high temperature favors the migration of Mn atoms away from interstitial and substitutional sites to be incorporated into the clusters as MnAs.

As outlined in Ref. 9, depending on the Mn concentration, the samples exhibit different magnetic behavior that can be linked to the size of the clusters. For the type I sample with a low Mn concentration of $x \leq 7.5\%$, the cluster diameters are small, ~6 nm, and have a zinc-blende crystal phase like the surrounding GaAs. The material has a low blocking temperature of $T_B = 10$ K. The blocking temperature characterizes the magnetic transition between two cluster states, i.e., superparamagnetism (the clusters are small ferromagnets, but they have a random magnetic moment orientation with respect to each other) and superferromagnetism (the ferromagnetic clusters have the same magnetic moment orientation). The type II sample with a high Mn concentration of $x > 7.5\%$ contains not only the same small clusters but also larger-sized clusters with diameters of roughly ~25 nm, which have a hexagonal NiAs crystal phase. T_B is well above room-temperature in this case. The two distinct crystal structures and the different magnetic behavior observed by the authors of Ref. 9 are connected to the X-STM results in the current article.

The X-STM measurements were performed on {110} GaAs surfaces in an Omicron room-temperature STM and in an Omicron low-temperature STM at $T = 77$ K, both operated under ultra-high vacuum (UHV) conditions with a base pressure of $p \leq 4 \times 10^{-11}$ mbar. The tips for the room-temperature STM were made from electrochemically etched pieces of polycrystalline W wire. The tips for the low-temperature STM were prepared each starting from a thin Cr rod that was electrochemically etched to obtain an atomically sharp apex. All tips were subsequently prepared in UHV by heating and Ar sputtering to remove contaminants and create more stability during measurements. Cr is antiferromagnetic, which makes tips of this material ideal for SP-STM, because they do not have a stray magnetic field but still show good magnetic sensitivity.[12,13] The electronic measurements of the band structure were performed by

a)e.p.smakman@tue.nl

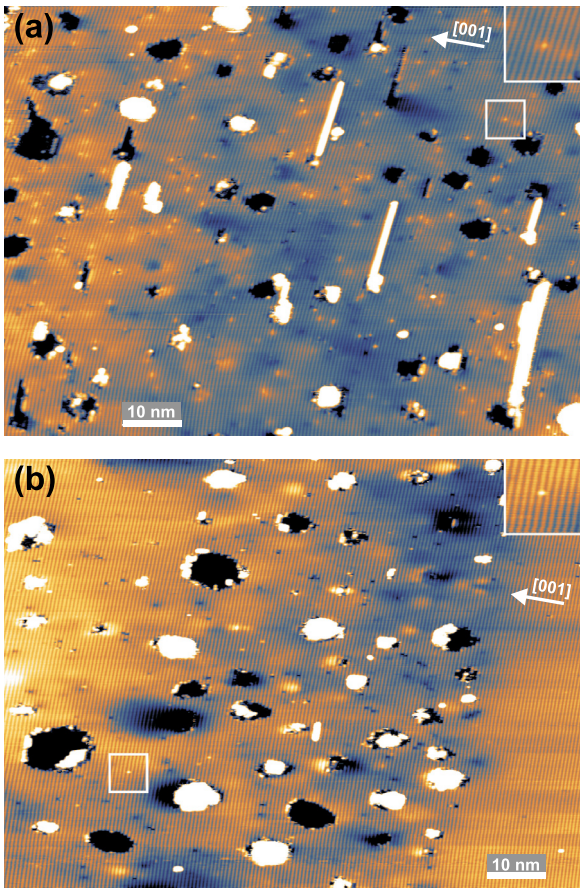

FIG. 1. $100 \times 74\,\text{nm}^2$ topographic images of (a) a type I sample and (b) a type II sample with MnAs clusters in GaAs. The insets show close-ups of single Mn dopants. $V = -2.70\,\text{V}$, $I = 40\,\text{pA}$. The white arrows indicate the growth directions.

directly taking *IV*-curves on the sample surface. The observations of magnetic switching were enabled by using an Ametek 5210 Dual Phase lock-in amplifier to obtain high-quality d*I*/d*V* information to probe the LDOS of the sample surface at a specific bias voltage.

In Fig. 1, X-STM images are displayed of the Be:GaMnAs epilayer of the type I and type II samples. In both figures, large structures are easily distinguished, which we link to MnAs clusters. There is no discontinuity of the crystal phase at the interface between the buffer layer and the Be:GaMnAs or for the interfaces inside the epilayer. Furthermore, small atomic-sized bright features are visible, also shown in the insets, which represent single Mn atoms in the GaAs matrix.[14] The Mn concentration is estimated by counting all the Mn atoms that are observed in the X-STM images. The Mn content in the Be:GaMnAs epilayer is found to be 0.7% for the type I and 0.9% for the type II sample. This is much lower than the initial Mn concentration, which indicates that Mn atoms migrate efficiently during the annealing step in order to form the MnAs nanoclusters. This is corroborated by the presence of very few As anti-sites compared to GaMnAs layers grown at the same growth temperature.[15] The total concentration of Mn is calculated by adding the single atom Mn concentration to the fraction of the area covered by the MnAs nanoclusters, resulting in 6.2% for the type I sample and 8.0% for the type II sample. These concentrations agree with the initial growth parameters for the two types of samples.[9]

The MnAs clusters give rise to both bright and dark contrasts with respect to the GaAs lattice. Because the metallic character corresponds to a good electrical conductivity, the MnAs appears brighter than the GaAs semiconductor in X-STM measurements. Besides that, in the case of the large-sized clusters, both protrusions and depressions arise because material is either left behind on or ripped out of the surface during the cleaving process, see Figs. 2(a) and 2(b). This occurs, for example, in areas where the crystal orientations of the materials do not match, as is expected for the MnAs in their hexagonal NiAs crystal phase. In Fig. 1(a), additional bright streaks are observed, which are monolayer cleaving artifacts, often originating from a cluster underneath. There is little outward relaxation visible in the GaAs directly surrounding the clusters, from which we conclude that there is a low amount of strain between the two materials. The combination of different crystal structures and low strain suggests a mechanical decoupling of GaAs and MnAs in the case of the large-sized clusters. Furthermore, neither structural defects in or near the MnAs material nor lattice deformations are visible, indicating that full relaxation occurs at the interfaces. For the small-sized clusters, in some cases, the zinc-blende crystal lattice structure is visible also in the MnAs and no protrusions or depressions related to the cleaving process are observed, see Fig. 2(c). From Ref. 9, the zinc-blende phase is expected to arise in the smaller nanostructures, which matches with the trend observed in the X-STM results. The larger clusters do not show atomic corrugation and also appear with larger height variations. We therefore assume that these larger clusters have the hexagonal NiAs phase.

In Fig. 3, histograms are displayed of the diameter distributions of the clusters for both type I and type II samples. The distributions were obtained from several X-STM images and are fitted with a normalized probability density function[16]

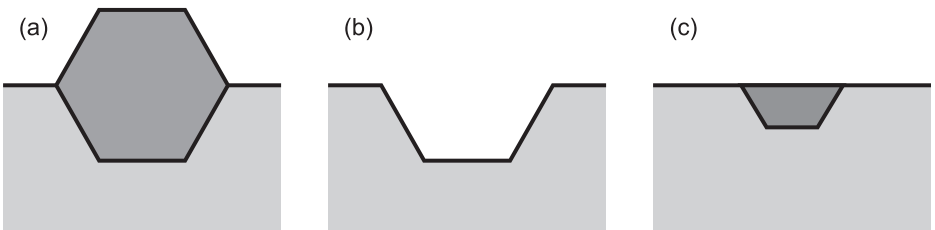

FIG. 2. Illustration of the MnAs clusters in GaAs after the cleaving process. Large clusters with the hexagonal NiAs crystal phase either (a) are left behind protruding from the surface or (b) are ripped out of the surface. (c) Small clusters with the zinc-blende crystal phase cleave along a {110} plane lined up with the surrounding GaAs.

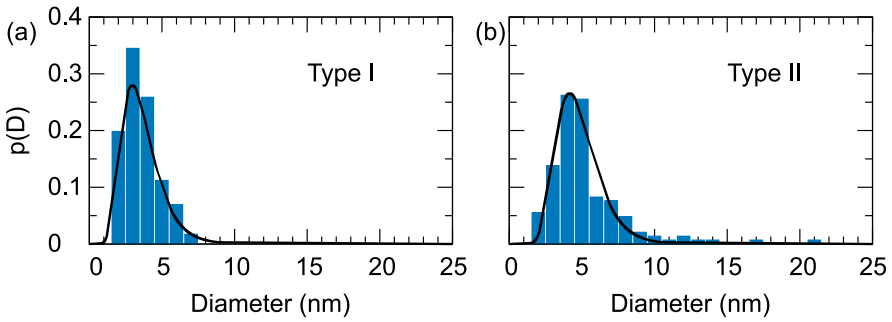

FIG. 3. Log-normal-fitted cluster size distributions for (a) the type I and (b) the type II samples.

$$p(D) = \frac{A}{\sigma D\sqrt{2\pi}} \exp\left[-\left(\frac{3\ln(D/D_0)}{\sigma\sqrt{2}}\right)^2\right], \qquad (1)$$

where D is the cluster diameter, D_0 is the median diameter of a cluster in the material, σ is the variance in the distribution, and A is a normalization factor. The fits result in $D_0 = 3.4$ nm for type I and $D_0 = 4.6$ nm for type II material. Furthermore, $\sigma = 1.1$ nm for type I and $\sigma = 0.9$ nm for type II material. These values agree with those found with transmission electron microscopy (TEM) studies discussed in Ref. 9. The histograms show that the size of the type I sample clusters is smaller than 8 nm, whereas in the type II sample clusters with a diameter larger than 20 nm were found. This confirms the appearance of a second class of larger-sized clusters when the Mn content in the initial Be:GaMnAs layer is increased.

In Fig. 4, the electronic band structure of a MnAs nanocluster is compared to the surrounding GaAs by plotting the dI/dV along the dashed white line visible in the corresponding topography image. The measurements were performed on a sample with a Mn concentration of $x = 7.5\%$. At the applied tunneling conditions, the contrast from electronic effects is suppressed in the height profile of the surface. This setting is therefore an appropriate starting condition for IV-spectroscopy, because it avoids cross-talk with the topography. Although MnAs is metallic, the nm size of the clusters results in a Coulomb blockade effect with an effective energy gap due to the charging of the cluster.[10] From the spectroscopic data, the charging energy can be estimated by intersecting the valence and conduction band edges with the electrical noise level on a semi-logarithmic scale. The charging energy of MnAs, $E_g = 0.20$ eV, is much smaller than the bandgap of GaAs, $E_g = 1.52$ eV. The electrostatic energy of a nanocapacitor is $e^2/2C$, where the capacitance is given by $C = 4\pi\epsilon_0\epsilon R$, with ϵ_0 the vacuum permittivity and $\epsilon = 1$ is the relative permittivity. The radius of the nanocluster is approximated at $R = 3.6$ nm, which matches well with the size observed in the topography measurement. Note that our choice for the value of ϵ assumes that the field distribution between the MnAs cluster and the STM tip is limited to the vacuum region. We expect that the deviations due to GaAs host dielectric properties are very small because only a very small portion of the field lines extend into the semiconductor host material for the MnAs clusters that reside at the vacuum-sample interface. Furthermore, the STM electronic noise level of ~1 pA results in a possible overestimation of the charging energy. The uncertainties in these two parameters have opposite effects: a larger effective ϵ decreases the estimated radius, while a lower STM electronic noise level could increase it. The charging energy measured with STM corresponds in order of magnitude to that observed in transport measurements performed on single MnAs nanoclusters in GaAs.[17]

The spin-polarized Cr tips that are used in the X-STM measurements have a magnetic sensitivity that is most apparent when recording dI/dV spectra. The switching of a zinc-blende MnAs cluster between two magnetizations is displayed in Fig. 5. The measurements were performed on a sample with a Mn concentration of $x = 7.5\%$. Because the current in this STM measurement is constant, only large abrupt changes are recorded in the signal, because in that case the feedback is too slow to adjust the tip height immediately. In our measurement, we observe a strong instability in the current at the position of the smaller-sized clusters. In the dI/dV signal, these regions correspond to areas where two distinct contrasts are observed. The signal switches between a dark and a bright contrast at random positions during scanning with the tip.

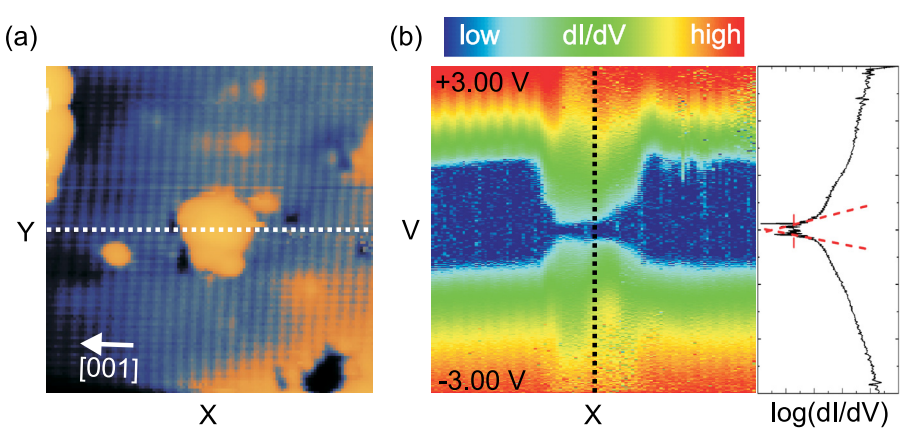

FIG. 4. (a) 12×12 nm^2 X-STM topography of a nanoscale MnAs cluster in GaAs, $V = -3.00$ V and $I = 100$ pA. The white arrow indicates the growth direction. (b) An IV-spectroscopy line spectrum, taken over the dashed white line indicated in the topography, 10 mV steps. The dI/dV is color-coded from blue (low) to red (high). The single dI/dV-spectrum is taken at the position indicated by the dashed black line and is displayed on a semi-logarithmic scale. The estimation of the bandgap is indicated by the dashed red lines. $T = 77$ K.

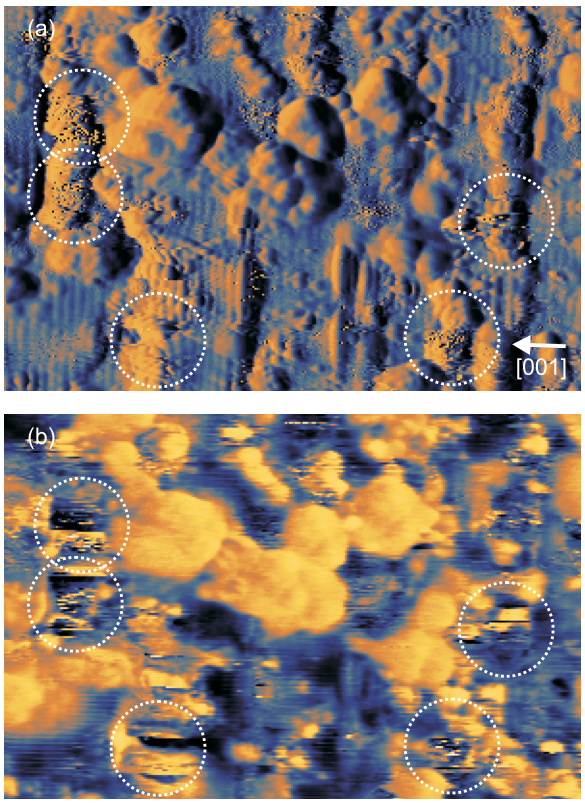

FIG. 5. $30 \times 20\,\text{nm}^2$ maps of (a) current and (b) dI/dV of switching zinc-blende MnAs nanoclusters in GaAs, $V = +1.25$ V, $I = 100$ pA, $V_{osc} = 35$ mV, $f_{osc} = 858$ Hz, and $\tau_{osc} = 3$ ms. The fast scan direction is left to right, the slow scan direction is bottom to top. The white arrow indicates the growth direction. The dotted white circles indicate the position of switching clusters. $T = 77$ K.

We argue that the two states in the dI/dV map correspond to two magnetic moments of the cluster, both along its magnetic easy axis but with opposite sign. The bistability originates from the magnetization reversal of a complete cluster, similar to Fe islands on a W surface described in Ref. 18. In (Ga,Mn)As samples, resistance noise measurements have been shown to exhibit random telegraph noise, corresponding to MnAs clusters with a magnetic moment of $m \sim 20\mu_B$.[19] The magnetization direction of the magnetic cluster is more parallel to that of the tip apex in the case of the bright contrast, and more anti-parallel when a dark contrast is observed.[20] This results in a different overlap between the spin local density of states (LDOS) of the tip and the sample for the opposite magnetization directions, giving a different contrast in the STM images. Because we have neither a magnetic field to direct the magnetization of our tip nor a reference sample with known magnetic orientations, we do not know the actual direction of magnetization in our measurements.

The magnetic switching occurs only for the smaller sized clusters, while the larger clusters remain stable. This suggests that the smaller clusters are superparamagnetic and do not contribute to the ferromagnetic state of the material. The larger clusters are not switching, suggesting superferromagnetic behavior under these conditions. This corresponds to the observations in Ref. 9, where the measured blocking temperature for material with on average smaller clusters is $T_B = 10$ K and that for material with on average larger

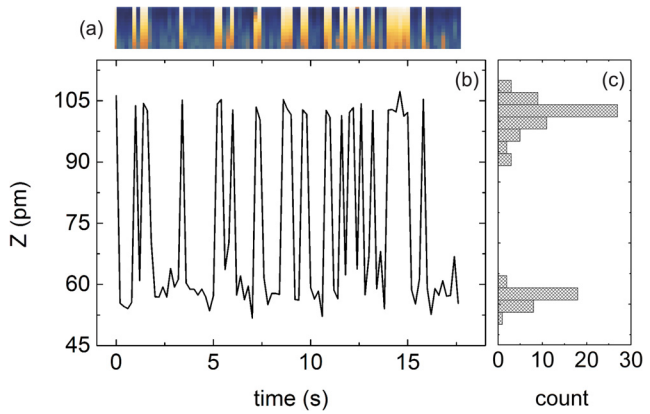

FIG. 6. The graph shows the random telegraph noise signal of a zinc-blende MnAs nanocluster in GaAs, $V = +1.75$ V and $I = 25$ pA. The corresponding 2 nm wide part of the topographic line trace is displayed on top. On the right, a histogram is shown of the tip height distribution during this measurement recorded in time, demonstrating the switching between two distinct states. $T = 77$ K.

clusters is above room-temperature. We chose the experimental temperature of $T = 77$ K in the X-STM measurements to verify the different magnetic behavior for the smaller and larger nanoclusters.

The magnetic sensitivity is most apparent in the dI/dV signal, but also translates into changes in the topography. Random telegraph noise of a single switching zinc-blende MnAs cluster observed in the topography is shown in Fig. 6. In this experiment, the tip was restricted to scan over a single line of 10 nm wide repetitively. From the resulting data set, the tip height in the center of a MnAs cluster is extracted as a function of time. The relative tip-sample distance for the two magnetic states with these tunneling conditions is on the order of 50 pm, which is well above the electrical and vibrational noise level of about 5 pm. A detailed study of the dynamical behavior of the switching is possible by varying the tunneling conditions, but this is outside of the scope of this work.

In summary, X-STM measurements confirm that the size of MnAs nanoclusters in GaAs is strongly dependent on the Mn content. The GaAs matrix exhibits a perfect strain-free zinc-blende crystal phase in the Be:GaMnAs epilayer. The clusters are composed of the zinc-blende crystal phase when they are small, but larger structures exhibit the hexagonal crystal structure. The Coulomb blockade effect observed in a small cluster matches with the size of the cluster and confirms the metallic character. The SP-STM measurements reveal that the smaller clusters switch between two distinct magnetic states, which means that they are superparamagnetic at $T = 77$ K, while the larger clusters do not switch and are superferromagnetic. This supports the view that larger sized clusters are needed to create stable ferromagnetism at room-temperature.

This work is part of the research program of the Foundation for Fundamental Research on Matter (FOM), which is part of the Netherlands Organization for Scientific Research (NWO), Grant No. 09NSE06. D.W.R. and N.S. acknowledge partial support through C-SPIN, one of six centers of STARnet, a Semiconductor Research Corporation program, sponsored by MARCO and DARPA.

[1]H. Ohno, Science **281**, 951 (1998).
[2]A. H. MacDonald, P. Schiffer, and N. Samarth, Nat. Mater. **4**, 195 (2005).
[3]D. D. Awschalom and M. E. Flatté, Nat. Phys. **3**, 153 (2007).
[4]T. Dietl, Nat. Mater. **9**, 965 (2010).
[5]M. Wang, R. P. Campion, A. W. Rushforth, K. W. Edmonds, C. T. Foxon, and B. L. Gallagher, Appl. Phys. Lett. **93**, 132103 (2008).
[6]J. De Boeck, R. Oesterholt, A. Van Esch, H. Bender, C. Bruynseraede, C. Van Hoof, and G. Borghs, Appl. Phys. Lett. **68**, 2744 (1996).
[7]M. Yokoyama, H. Yamaguchi, T. Ogawa, and M. Tanaka, J. Appl. Phys. **97**, 10D317 (2005).
[8]S. Kuroda, N. Nishizawa, K. Takita, M. Mitome, Y. Bando, K. Osuch, and T. Dietl, Nat. Mater. **6**, 440 (2007).
[9]D. W. Rench, P. Schiffer, and N. Samarth, Phys. Rev. B **84**, 094434 (2011).
[10]B. Rache Salles, J. C. Girard, C. David, F. Offi, F. Borgatti, M. Eddrief, V. H. Etgens, L. Simonelli, M. Marangolo, and G. Panaccione, Appl. Phys. Lett. **100**, 203121 (2012).
[11]B. Grandidier, J. P. Nys, C. Delerue, D. Stiévenard, Y. Higo, and M. Tanaka, Appl. Phys. Lett. **77**, 4001 (2000).
[12]A. Li Bassi, C. S. Casari, D. Cattaneo, F. Donati, S. Foglio, M. Passoni, C. E. Bottani, P. Biagioni, A. Brambilla, M. Finazzi, F. Ciccacci, and L. Duò, Appl. Phys. Lett. **91**, 173120 (2007).
[13]A. Schlenhoff, S. Krause, G. Herzog, and R. Wiesendanger, Appl. Phys. Lett. **97**, 083104 (2010).
[14]A. M. Yakunin, A. Y. Silov, P. M. Koenraad, J. H. Wolter, W. Van Roy, J. De Boeck, J.-M. Tang, and M. E. Flatté, Phys. Rev. Lett. **92**, 216806 (2004).
[15]S. J. C. Mauger, M. Bozkurt, P. M. Koenraad, A. D. Giddings, R. P. Campion, and B. L. Gallagher, Phys. Rev. B **84**, 104432 (2011).
[16]A. Kwiatkowski, D. Wasik, P. Dłużewski, J. Borysiuk, M. Kamińska, A. Twardowski, and J. Sadowski, J. Magn. Magn. Mater. **321**, 2788 (2009).
[17]P. N. Hai, S. Ohya, and M. Tanaka, Nat. Nanotechnol. **5**, 593 (2010).
[18]S. Krause, L. Berbil-Bautista, G. Herzog, M. Bode, and R. Wiesendanger, Science **317**, 1537 (2007).
[19]M. Zhu, X. Li, G. Xiang, and N. Samarth, Phys. Rev. B **76**, 201201 (2007).
[20]R. Wiesendanger, H.-J. Güntherodt, G. Güntherodt, R. J. Gambino, and R. Ruf, Phys. Rev. Lett. **65**, 247 (1990).